Journal of Optics
https://doi.org/10.1007/s12596-024-02154-9

RESEARCH ARTICLE

# A simple method to prepare and characterize optical fork-shaped diffraction gratings for generation of orbital angular momentum beams

**Mohammad Reza Rashidian Vaziri[1,2] · Abolfazl Hosseini[3] · Ebrahim Gholami Hatam[3] · Reza Azmoodeh Sorodi[4,5]**

Received: 14 July 2024 / Accepted: 5 August 2024


**Abstract**
In this paper, a simple method is reported for the design and preparation of fork-shaped diffraction gratings with different topological charges. First, the diffraction gratings were prepared using the computer-generated holography technique. Using the image processing methods in the MATLAB environment, the images of the generated holograms were first prepared in the gray level format, then converted into binary, and finally saved in the vector form. The vector images prepared from the holograms were printed on transparent sheets using a semi-industrial printer. By optimizing the groove distance of the gratings through experimental tests, the groove distance equal to 175 micrometers has been chosen as the optimal line distance for making the gratings. By designing and setting up a suitable optical arrangement, the prepared fork-shaped gratings were exposed to laser beams and Laguerre-Gaussian beams were generated. The results showed the desired generation of these types of beams with the simple method presented for making the gratings. In the following, by setting up a Mach-Zehnder interferometric setup, the topological charges of the generated Laguerre-Gaussian beams were also measured. The results indicated that the number of fork branches formed in the interference patterns was equal to the topological charge of the Laguerre-Gaussian beams. Using computer simulations, the experimental results obtained in this work have also been examined and tested.

**Keywords** Optical diffraction · Computer-generated holography · Orbital angular momentum · Quantum communications

## Introduction

In recent years, the application of laser beams with non-Gaussian transverse intensity distributions has been of considerable interest. Beams with Top Hat, Bessel-Gaussian, Laguerre-Gaussian, and Hermit-Gaussian intensity distributions are of great interest in this area. Among the beams with non-Gaussian intensity distributions, Laguerre-Gaussian beams carry orbital angular momentum, which can increase the bandwidth of information transmission in optical communication [1, 2]. In fact, spin angular momentum is not the only type of angular momentum that an electromagnetic wave may carry along its propagation path. Like other particles, photons can also have orbital angular momentum. A transverse component of the photon's linear momentum can lead to the generation of angular momentum in the propagation direction [3].

✉ Mohammad Reza Rashidian Vaziri
rashidianvaziri@um.ac.ir

1 Department of Physics, Faculty of Sciences, Ferdowsi University, Mashhad, Iran

2 Photonics and Quantum Technologies Research School, Nuclear Science and Technology Research Institute, Tehran, Iran

3 Department of Physics, Faculty of Science, Malayer University, Malayer, Iran

4 Department of Physics, Faculty of Basic Sciences, Tarbiat Modares University, Tehran, Iran

5 Iranian National Center for Laser Science and Technology, Hashtgerd, Iran

Published online: 22 August 2024

In this study, we focus on the generation of Laguerre-Gaussian beams with specific properties. Laguerre-Gaussian beams are characterized by their azimuthal phase variation and carry orbital angular momentum. The optical field of a Laguerre-Gaussian beam can generally be expressed as [4]

$$LG_p^{(l)}(r,\varphi,z) = A_0(r,z)\exp(il\varphi) \tag{1}$$

where $A_0(r, z)$ is defined as

$$\begin{aligned} A_0(r,z) = &\sqrt{\frac{2p!}{\pi(p+|l|)!}}\frac{1}{w(z)}\left[\frac{r\sqrt{2}}{w(z)}\right]^{|l|} L_p^{(|l|)}\left[\frac{2r^2}{w^2(z)}\right] \\ &\exp\left[-\frac{r^2}{w^2(z)}\right]\exp\left[\frac{ikr^2z}{2(z^2+z_R^2)}\right] \\ &\times\exp\left[-i(2p+|l|+1)\tan^{-1}\left(\frac{z}{z_R}\right)\right] \end{aligned} \tag{2}$$

where $z$ represents the distance between the input plane and the receiver plane, $r$ is the radial coordinate in a polar coordinate system. $l$ and $p$ denote the topological charge and radial index, respectively. $w(z) = w_0\sqrt{1+(z/z_R)^2}$ is the beam width at distance (z), $w_0$ is initial beam width (fundamental Gaussian beam radius), $z_R = \pi w_0^2/\lambda$ is the Rayleigh range, $k = 2\pi/\lambda$ is the wave number, $\lambda$ is the wavelength, and $L_p^{(|l|)}(.)$ is the associated Laguerre polynomial. Specifically, we are interested in beams with zero radial index ($p = 0$, i.e., no radial variation) and a non-zero azimuthal index ( $l$ ). These beams exhibit a helical wavefront and possess unique properties due to their OAM. By controlling the azimuthal index, one can tailor the beam's intensity profile and phase structure, making them valuable for various applications.

Various methods have been used for generation of Laguerre-Gaussian beams so far. For the first time, it was shown by Allen and his colleagues that a beam with a spiral phase front has a certain amount of orbital angular momentum [5]. To convert the Hermite-Gaussian modes into the Laguerre-Gaussian ones, they used a set of precisely-aligned cylindrical lenses. Another method for generation of orbital angular momentum beams was based on the use of a new tool called spiral phase plate to induce the spiral phase fronts on the impinging beams [5]. The spiral phase plate is an optical component that is made of glass with an optical thickness that increases with the azimuthal angle [6]. Due to this structural feature, when a uniform plane wavefront beam passes through this component, it transforms into a spiral wavefront. Another method has also been developed that creates a topological charge in the phase front of a beam, depending on the primary polarization state of the beam [7]. At the heart of this process is an anisotropic birefringence plate, which is made of liquid crystal and has a well-defined topological charge in the transverse plane, which is known as the q-plane. Computer-generated holography also provides another method to generate the Laguerre–Gaussian beams that carry orbital angular momentum [8]. If an oblique spiral beam interferes with a plane-wave reference beam, the resulting interference pattern will be called a fork-shaped hologram. This hologram can be used for generation of an orbital angular momentum beam. When the fork-shaped hologram is illuminated by a $TEM_{00}$ beam, the original optical power is transferred to the diffraction orders. In the first two diffraction orders, spiral beams with opposite signs of angular momentum will be generated. Due to the availability of commercial spatial light modulators (SLM), the transferred computer-generated holograms to these devices are now being widely used for real-time generation and detection of orbital angular momentum beams [9, 10]. Fork-shaped gratings can be prepared using straightforward computer-generated holography techniques [11]. Unlike some other methods that require complex optical setups or specialized components, they can be fabricated using standard laboratory equipment [12]. Fork-shaped gratings can also produce different optical vortex beams in different diffraction orders, allowing for versatility in applications [13]. These advantages make fork-shaped gratings a compelling choice for generating optical vortex beams in various contexts.

Due to their unique features, the orbital angular momentum beams have been used in various fields. As one of the first applications, the orbital angular momentum carrying Laguerre–Gaussian beams were used for rotation and aligning of microscopic objects [14]. Some years later, the first clear demonstration of the transfer of orbital angular momentum of light to microscopic objects with optical tweezers was taken place [15]. Apart from the classical applications, the orbital angular momentum of light is also favored from the quantum viewpoint. Spin angular momentum is inherently a binary quantity and hence, only one bit of information can be encoded in the photon carrying this type of momentum. However, orbital angular momentum has infinite degrees of freedom. Therefore, more alphabets are available for writing in the orbital angular momentum space. It is shown that the multidimensionality of the orbital angular momentum space can be used for encoding information in free space communications [2]. Detection, high-resolution microscopy, quantum cryptography, radio telecommunications, and optical communication based on free space propagation and in optical fibers are other applications of angular momentum beams [5, 16, 17].

In this paper, the design, preparation, and characterization of fork-shaped diffraction gratings with different topological charges have been reported. The gratings have been prepared in a simple and reproducible way using computer-generated holography and their groove distance has been optimized. In the following, the functional capabilities of

the prepared gratings have been investigated using suitable optical arrangements. By computer simulations, the obtained experimental results in this work have also been examined and tested.

## Methods

### Design of fork-shaped gratings by computer-generated holography

With the advancement of computer technology and related devices such as digital printers, the computer-generated holography field has greatly progressed in the last decade since with a computer, the hologram of any object can be calculated, even if this object does not exist externally [18]. In this work, the computer holograms have been designed by calculating and plotting the interference patterns resulting from the superposition of an inclined plane wave and Laguerre–Gaussian waves. According to the holography theory, if this computer hologram is made physically and is illuminated by the primary plane wave beam, the Laguerre–Gaussian waves will be reconstructed and exit from the other face of the hologram. The general form of a plane wave can be written as:

$$E_1 = e^{-i\vec{k}.\vec{r}} \tag{3}$$

where $\vec{k}$ is the wave vector and $\vec{r}$ is the position vector. Consider the wave vector of the inclined plane wave as $\vec{k} = k_x \vec{i} + k_z \vec{k}$ (to simplify the expression, the y component is omitted), this plane wave can be written as follows:

$$E_1 = e^{-i(k_x x + k_z z)} \tag{4}$$

The Laguerre–Gaussian beam equation can also be written in the following simple form:

$$E_2(r, \theta, z) = E_0 e^{il\theta} e^{-ik_z z} \tag{5}$$

where $l$ represents the topological charge of the optical vortex and $\theta = tg^{-1}(y/x)$ is the azimuthal angle. Using Eqs. (3) and (4), the superposition of these two waves can be expressed mathematically as [19]:

$$H = 1 + |E_0|^2 + 2|E_0| \cos(k_x x - l\theta) \tag{6}$$

The component of the wave vector in the x direction can be written as follows:

$$k_x = \frac{2\pi}{\Lambda} \tag{7}$$

Which $\Lambda$ is the spatial periodicity of the formed interference pattern, or the groove distance when it is used as a diffraction grating. Using the relation $x = r\cos\theta$, Eq. (5) converts into the following form:

$$H = 1 + |E_0|^2 + 2|E_0| \cos\left(\frac{2\pi}{\Lambda} r\cos\theta - l\theta\right) \tag{8}$$

Equation (6) represents an amplitude hologram. The constant terms and coefficients can be omitted to be able to convert it to the following simpler form:

$$H = \cos\left(\frac{2\pi}{\Lambda} r\cos\theta - l\theta\right) \tag{9}$$

In comparison with the amplitude holograms that modulate the amplitude of the incident light, phase holograms modulate the phase of light and leave the amplitude unchanged. Because the intensity of the light transmitted through the hologram is proportional to the square of the modulus of the amplitude and not the phase, the phase holograms are ideally without absorption and the diffracted light from them has higher intensities and hence is more applicable. To convert the amplitude hologram (9) into a phase hologram, it is enough to put the corresponding term in the argument of an exponential function:

$$PH = e^{-iH} = e^{i\cos\left(l\theta - \frac{2\pi}{\Lambda} r\cos\theta\right)} \tag{10}$$

This equation has been used to create the computer-generated holograms in this work. The topological charge or the order of the generated Laguerre-Gaussian mode is determined by the integer parameter $l$. The groove distance is also determined by the parameter $\Lambda$.

### Image binarization and preparation of the gratings

Binary images are widely used in image processing and almost most of the images must be converted to these types of images before further processing. To convert a gray-level image to a binary image, the intensity values between 0 and 256 for each pixel must be converted to values between 0 and 1. For this, a threshold limit should be defined, in such a way that values less than this threshold limit are replaced by zero, and values greater than it are replaced by one. If $f(x, y)$represents the gray image matrix and $g(x, y)$be its equivalent binary image matrix, they are related as follows:

$$g(x, y) = \begin{cases} 1 & \text{if } f(x, y) \geqslant T \\ 0 & \text{if } f(x, y) < T \end{cases} \tag{11}$$

where $T$ is the threshold limit. Therefore, using this mathematical relation for each pixel of a gray-level image, it can be converted to a binary. There are different methods to determine the threshold value. The best way to convert an image into binary is to determine the value of the threshold limit using the histogram of the image and its final optimization by trial and error. In this work, by trial and error, the threshold limit equal to 0.6 has been found and used as the optimal limit for producing the same width of black and white lines in the binary images of the fork-shaped gratings.

In this work, generation of computer-generated holograms and their binarization is performed in the MATLAB environment. To be able to print and transfer such digital binary images on the surface of transparent sheets, they must first be appropriately stored in the computer memory. Digital images can be stored as vector or raster formats. Raster images are composed of tiny squares called pixels. These pixels collectively form detailed images, such as photographs. When one zoom in on a raster image, sees individual pixels, which can make the image appear grainy or blurry. Indeed, Raster images lose quality when resized because the pixel grid remains fixed. Vector images, on the other hand, use mathematical equations to define shapes, lines, and curves. There are no pixels in a vector file. The beauty of vector images lies in their scalability. One can resize, rescale, and reshape them infinitely without any loss of quality. Their resolution remains consistent regardless of size changes [20]. Since it is sometimes necessary to resize and zoom the images during the transfer process, to avoid the usual blurring of pixel images during such enlargements, the images have been saved in the vector form using the export_fig code. This code has been developed to avoid the common errors that sometimes occur during the storing of digital images in MATLAB [21]. This user-friendly code allowed us to convert our grayscale images (which are initially raster-based) into vector format. By exporting the images as vectors, we ensured that their quality would remain intact even when resized, which is crucial for our high-resolution printing process. Finally, a commercial digital printer (model HP LaserJet Enterprise M806DN) was used to transfer the binary vector images on the surface of transparent sheets.

## Simulation of Gaussian Beam diffraction from the fork-shaped diffraction gratings

For generation of Laguerre–Gaussian beams, usually, a laser beam with Gaussian spatial distribution is irradiated on the surface of fork-shaped gratings. The Laguerre–Gaussian beams are formed due to optical diffraction and become visible in the far field. Therefore, in simulating the generation of Laguerre–Gaussian beams, the Fraunhofer diffraction of the incident Gaussian beam from the fork-shaped gratings plays the leading role. As mentioned in section Design of fork-shaped gratings by computer-generated holography, the fork-shaped diffraction gratings are designed by mathematically interfering an oblique plane wave with Laguerre–Gaussian beams. Therefore, to simulate the diffraction from the designed fork-shaped gratings, a plane wave must be irradiated on the surface of these gratings. However, due to the similarity of the far-field Gaussian beam wavefront with the plane wave, the Gaussian beam can also be used for this purpose. The mathematical calculation of this process is done by multiplying the Gaussian beam wave function by the fork-shaped diffraction function, Eq. (9), and performing the Fourier transform of the resulting product [22, 23]:

$$I = F\left(\Psi_1 \times PH\right) \tag{12}$$

where $I$ indicates the intensity distribution in the viewing plane, $\Psi_1$ is the Gaussian beam wave function and $PH$ is the fork-shaped grating function. To simulate this process, the fast Fourier transform algorithm is used in the MATLAB environment. The Fourier transformation yields the Fraunhofer diffraction orders, which will be different depending on the magnitude of the topological charge of the fork-shaped grating.

## Measurement of the topological charges

As mentioned in section Design of fork-shaped gratings by computer-generated holography, the superposition of a Laguerre–Gaussian beam with a certain topological charge with an oblique plane wave will lead to the formation of a fork-shaped diffraction grating whose number of branches is exactly equal to the magnitude of the topological charge. Now, suppose that we have a Laguerre–Gaussian beam whose topological charge, which is equal to the magnitude of the angular momentum of its photons, is unknown. The interferometry technique is usually used for measuring the magnitude of the unknown topological charge of a Laguerre–Gaussian beam. By interfering this Laguerre–Gaussian beam with a plane wave and by counting the number of fork branches formed in the resulting interference pattern, the magnitude of the topological charge of the Laguerre–Gaussian beam can be easily determined. In this work, the experimental interferometer setup, whose design is shown in Fig. 1, is used to measure the magnitude of the topological charge of the generated Laguerre–Gaussian beams. In this setup, the two reference and object beams are produced by irradiating the cubic beam splitter with a He-Ne laser beam (Melles Griot 3225 H-PC, 632.8 nm, 10 mW). The first beam creates the diffraction pattern including the Laguerre–Gaussian beams after hitting the fork-shaped

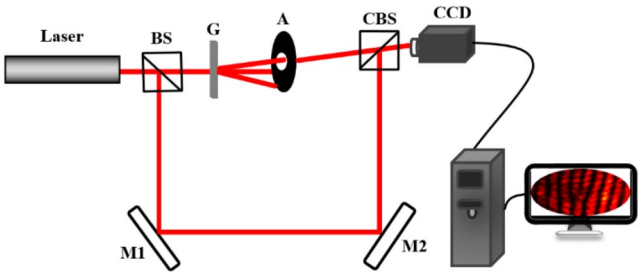


**Fig. 1** The Mach-Zehnder interferometric setup used to measure the topological charge of the Laguerre–Gaussian beams

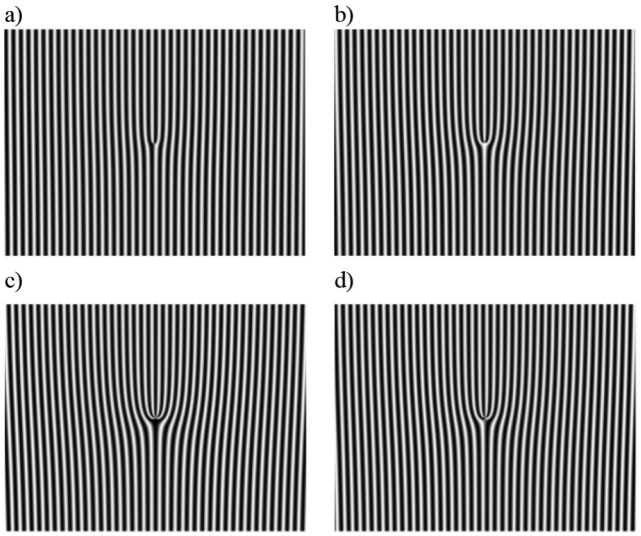


**Fig. 2** The designed fork-shaped diffraction gratings with different values of topological charge equal to (**a**) 1, (**b**) 2, (**c**) 3, and (**d**) 4

diffraction grating. The first order of diffraction is separated from the pattern by a circular aperture and the other orders are blocked. The separated diffraction order, i.e. the Laguerre–Gaussian mode, reaches the surface of the CCD (DMK23G445, The imaging source) after passing through the second beam splitter (the combining beam splitter). The reference beam also reaches the light-sensitive surface of the CCD after two consecutive reflections from the flat mirrors and one more reflection from the combining beam splitter. The CCD records the interference pattern resulting from the superposition of these two beams and transfers it to the computer. By counting the number of fork branches in the resulting interference pattern, the topological charge of the Laguerre–Gaussian beam can be measured.

## Results

Figure 2 shows the fork-shaped diffraction gratings designed by computer-generated holography with topological charges equal to 1 to 4. As can be verified, the number of fork branches in each case is equal to the topological charge

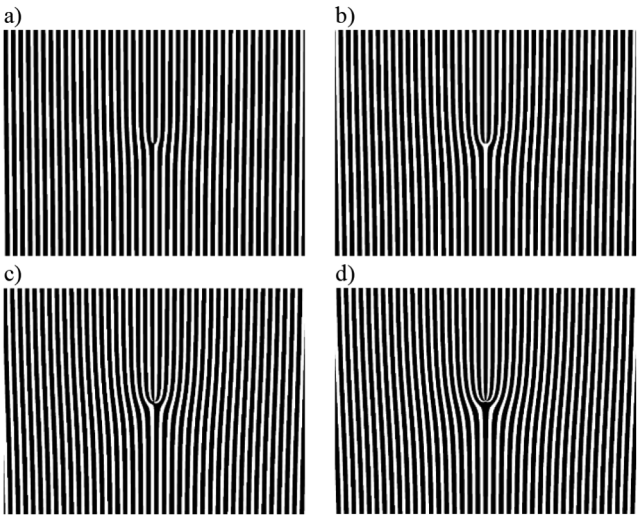


**Fig. 3** The binary form of the fork-shaped diffraction gratings shown in Fig. 2

of the Laguerre–Gaussian beam that is used in the design of the hologram.

The shown images in Fig. 2 are gray-level images. Therefore, the visible black and white fringes in these images are not completely black and white at every point. This means that, for example, the black fringes have values between 0 and 256, and when moving from a black fringe to its adjacent white fringe, the intensity of the image pixels varies between these values. Printing such images by digital printers that only have the states of zero and one (without ink and with ink), will yield the gratings that the distance between their lines is different from what is considered in their design phase. For this reason, the gray-level images of the gratings have been binarized using the method mentioned in section Image binarization and preparation of the gratings. Figure 3 shows the binary images of the fork-shaped diffraction gratings.

After preparation of the binary images and their vectorization, they have been transferred to the CorelDraw graphics software environment. In this software, the dimensions of the page were adjusted according to the dimensions of an A4 paper and the imported images were placed next to each other in a mosaic form. In this way, it is possible to obtain a larger number of diffraction gratings with different topological charges with a single print.

When a laser beam impinges normally on the surface of a diffraction grating, the angular separation distance between the different diffraction orders is inversely proportional to the distance between the grating lines (or the groove distance). Therefore, if the groove distance is reduced, the angular separation distance between the diffracted output beams from the fork-shaped grating will increase. It should be noted that in preparation of diffraction gratings,

it is desirable to have the smallest groove distance, since in applications that require the use of these gratings these diffracted beams will not interfere with each other at short distances from the gratings. However, the groove distance cannot be reduced unlimitedly. In practice, the minimum value of the groove distance is limited by the resolution of the method used for preparation of the grating. The printer used for preparation of the fork-shaped gratings was semi-industrial and of high quality, capable of printing with a real resolution of 1200 dpi. However, it should be noted that this resolution depends on variables such as the type of paper used for printing, the life of the cartridge, etc. In this work to obtain the desired gratings with the smallest groove distance, first, only the gratings with the topological charge of one and with different groove distances from 150 micrometers to 250 micrometers with 25 micrometer steps were prepared. After preparation, their surface have been investigated by an optical microscope. In order to check the conformity of the groove distances obtained after the preparation with the ones considered initially in the design phase of the gratings, the groove distances have been measured using the taken optical microscope images.

The measured groove distances and their comparison with the ones considered in the design phase are presented in Fig. 4. It should be kept in mind that in the ideal case, the graph should have a linear shape corresponding to the bisector of the first quadrant of the Cartesian coordinate system. Indeed, if the graph matches with the bisector of the first quadrant, exactly the same distance that is considered in the design phase is obtained in the experimental phase and after the preparation of the gratings. However, in practice, the lack of coordination between the printer software and the software containing the graphic files results in the difference between what is considered in the design phase and the ones obtained in the preparation phase. To continue the work, the smallest groove distance that yields a suitable resolution in the microscopic images should be selected. Keeping this condition in mind, the optimal groove distance of 175 micrometers has been selected for the preparation of other fork-shaped diffraction gratings.

After the determination of the optimal groove distance, fork-shaped gratings with topological charges of 1 to 4 have been prepared using this optimal distance. Figure 5 shows the optical microscope images of the prepared fork-shaped gratings.

To characterize the gratings, generation of Laguerre–Gaussian beams after laser light diffraction from them has been studied using the experimental setup shown in Fig. 6. In this arrangement, a helium-neon laser with linear polarization output is used. In order to avoid the occurrence of thermal effects in the grating, a polarizer has been used to adjust and decrease the incident laser power. The light is

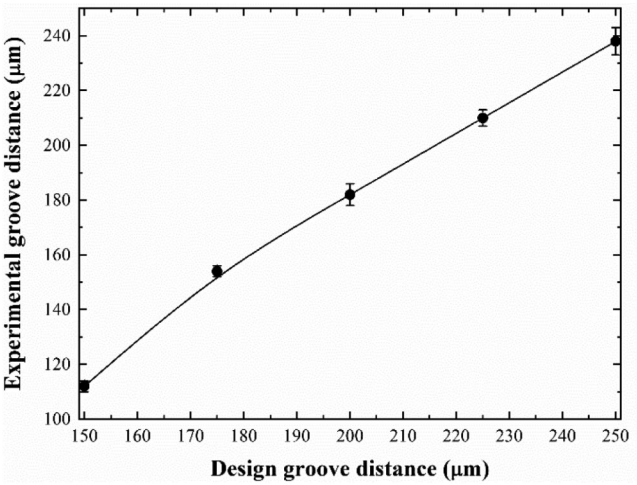


**Fig. 4** The measured experimental groove distance for the gratings made with the topological charge of one versus the groove distance considered in their design phases

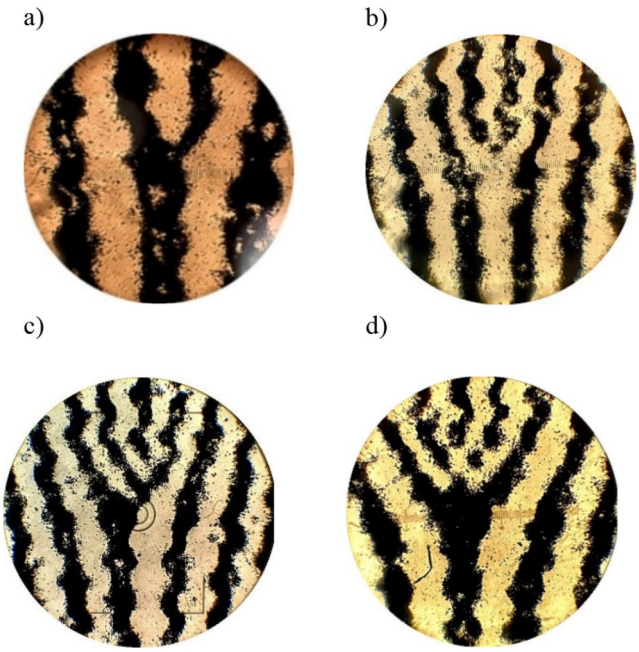


**Fig. 5** Optical microscope images of fork-shaped gratings with the groove distance of 175 micrometers and topological charges equal to (**a**) 1, (**b**) 2, (**c**) 3, and (**d**) 4

directed by a flat mirror towards the grating, which is placed inside the holder. The diffracted light from the grating is imaged by a convex lens with a focal length of 7 cm on the CCD camera. The images are recorded by the camera and transferred to the computer in real-time. Figure 7 shows the images of the recorded diffraction patterns of the fork-shaped gratings. The central intense circular pattern in the figures is the result of zero-order diffraction, which must have the original Gaussian distribution of the used laser beam. However, due to some overlap with its adjacent next

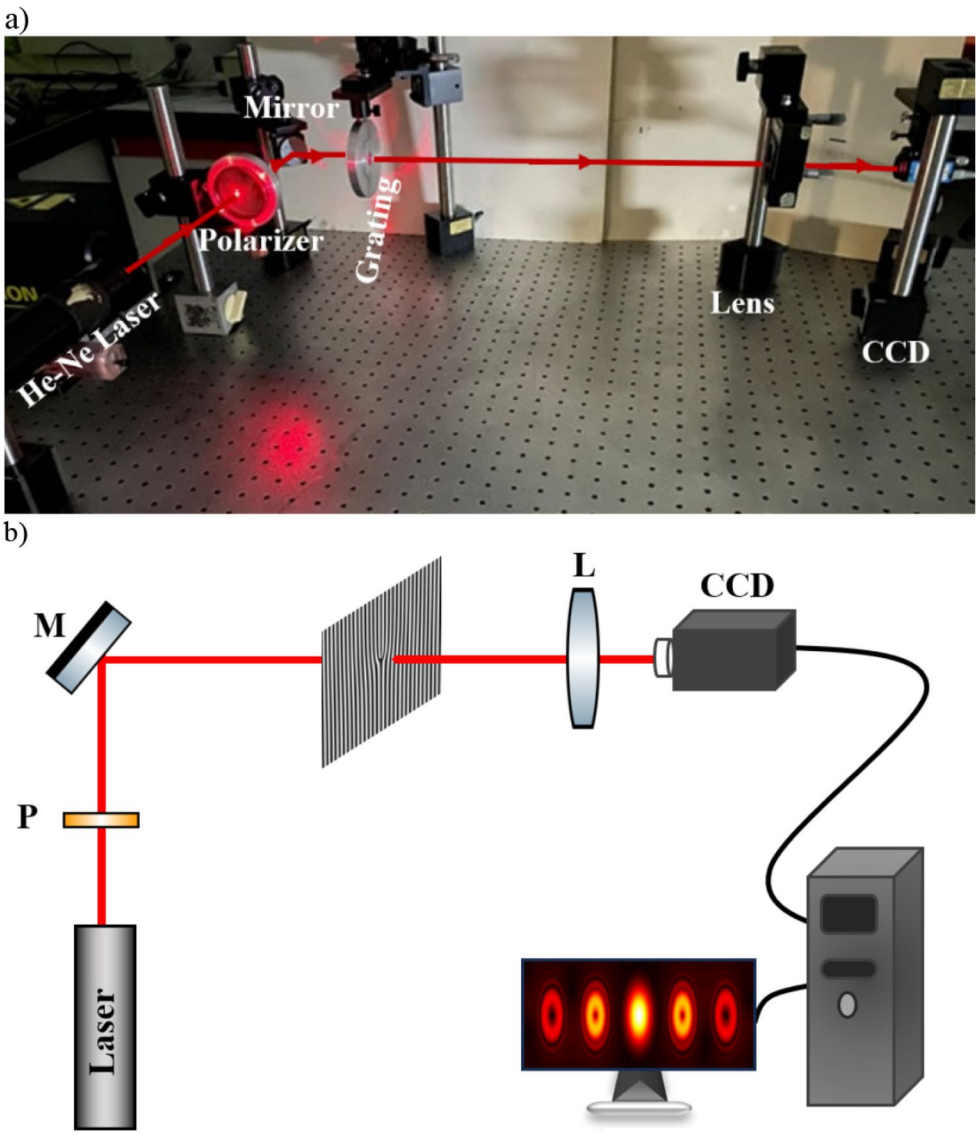


**Fig. 6** (**a**) Experimental setup used for generation of Laguerre–Gaussian beams. (**b**) Schematic representation of the setup (P: polarizer, M: flat mirror, and L: imaging lens)

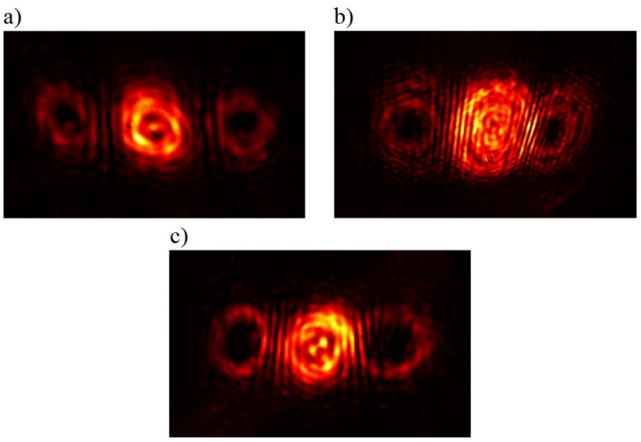


**Fig. 7** Diffraction patterns recorded for fork-shaped gratings with topological charges equal to (**a**) 1, (**b**) 2 and (**c**) 3

orders of diffraction, the Gaussian distribution has been somewhat changed.

Hollow circular intensity distributions indicate the produced first-order Laguerre–Gaussian modes, which are also known as donut modes or optical vortices. The topological charges of these modes have opposite signs. At the distance where the digital camera was placed, the transverse distributions of the diffraction orders have slightly overlapped. The diffraction orders appear as concentric rings with a dark spot at the center. The number of rings corresponds to the topological charge of the grating. These patterns are symmetric with respect to the center of the grating. The intensity of the diffracted beams decreases with increasing diffraction order. The diffraction efficiency of the gratings is approximately 29%. However, this efficiency decreases with higher topological charges of the grating. These findings are consistent with previous studies [5, 6], which also observed

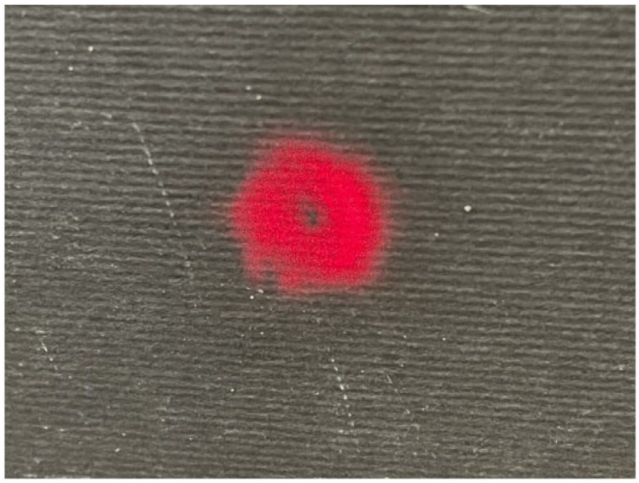

**Fig. 8** The separated Laguerre–Gaussian beam from the diffraction pattern of a fork-shaped grating with a topological charge equal to 1 by an adjustable aperture

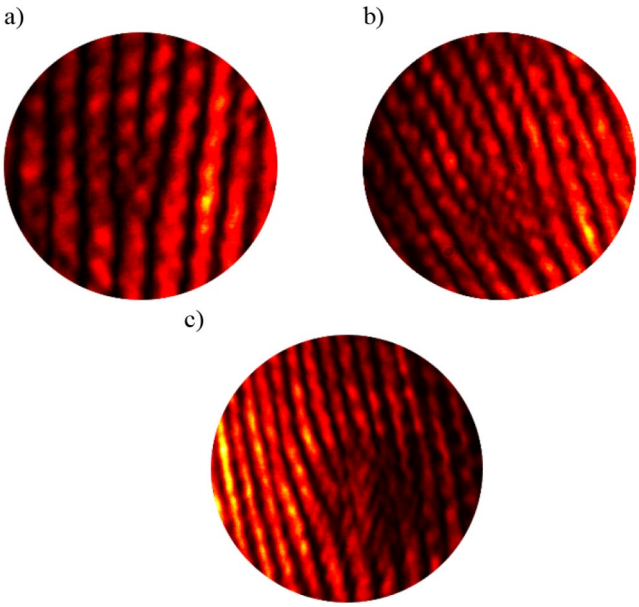


**Fig. 9** The interference patterns obtained for Laguerre-Gaussian beams with topological charges equal to (**a**) 1, (**b**) 2, and (**c**) 3

similar diffraction patterns and efficiencies for fork-shaped gratings.

By removing the CCD from the optical setup in Fig. 6 and recording the diffraction patterns at far distances, more than 3 m for the prepared gratings in this work, the first diffraction order can be separated from the rest by an adjustable aperture (Fig. 8). The separated Laguerre-Gaussian beams in this way can be used in applications that require the use of this type of beams.

Reinspecting Fig. 7, it is obvious that is impossible to determine the topological charge of the Laguerre–Gaussian beams from their transverse intensity distributions. To measure the topological charge of generated Laguerre–Gaussian beams, the interferometer arrangement shown in Fig. 1 is used. Figure 9 shows the recorded interference patterns for different Laguerre–Gaussian beams. As mentioned earlier, by counting the number of fork branches formed in each pattern, the magnitude of the topological charge of its corresponding Laguerre–Gaussian beam can be obtained. Indeed, when a Laguerre–Gaussian beam with a topological charge $l$ interferes with a plane wave, the phase singularity of the beam causes a dislocation in the interference fringes. This dislocation manifests as a fork-shaped pattern, where the number of branches in the fork is equal to $|l|$. The results are consistent with the findings reported in similar studies on the topic [1, 2].

In section Simulation of Gaussian beam diffraction from the fork-shaped diffraction gratings, the method of simulating the diffraction of a Gaussian beam (or a plane wave) from fork-shaped diffraction gratings has been described. Figure 10 shows the effect of changing the groove distance of the fork-shaped gratings in changing the obtainable far-field diffraction patterns when the Gaussian beam hits the surface. As can be verified, by decreasing the groove distance, the separation distance between the different diffraction orders increases. The zero-order diffraction in the center of the images is actually the original Gaussian beam that exits the grating without diffraction. Diffraction orders of $+1$ and $-1$ indicate the Laguerre–Gaussian beams with topological charges of $+1$ and $-1$. Diffraction orders of $+2$ and $-2$ also indicate the Laguerre–Gaussian beams with topological charges of $+2$ and $-2$. The important point is that with increasing the diffraction order, its intensity gradually decreases so that in the present simulation the diffraction orders of $+3$ and $-3$ are invisible. In experimental conditions, it is difficult to record the low-intensity diffraction orders and as can be verified in Fig. 7, diffraction orders higher than $+1$ and $-1$ cannot be seen for the gratings made in this work.

In Fig. 11, the effect of variation of the beam waist of the irradiated Gaussian beam on the surface of a fork-shaped grating in changing its far-field diffraction patterns is investigated. As can be seen in the figure, by reducing the waist size, Laguerre–Gaussian beams with a larger cross-sectional area can be obtained at a specified distance. This result can be justified by considering the fact that for a Gaussian beam, by reducing the waist size larger spot sizes will be obtained upon propagation due to the natural diffraction.

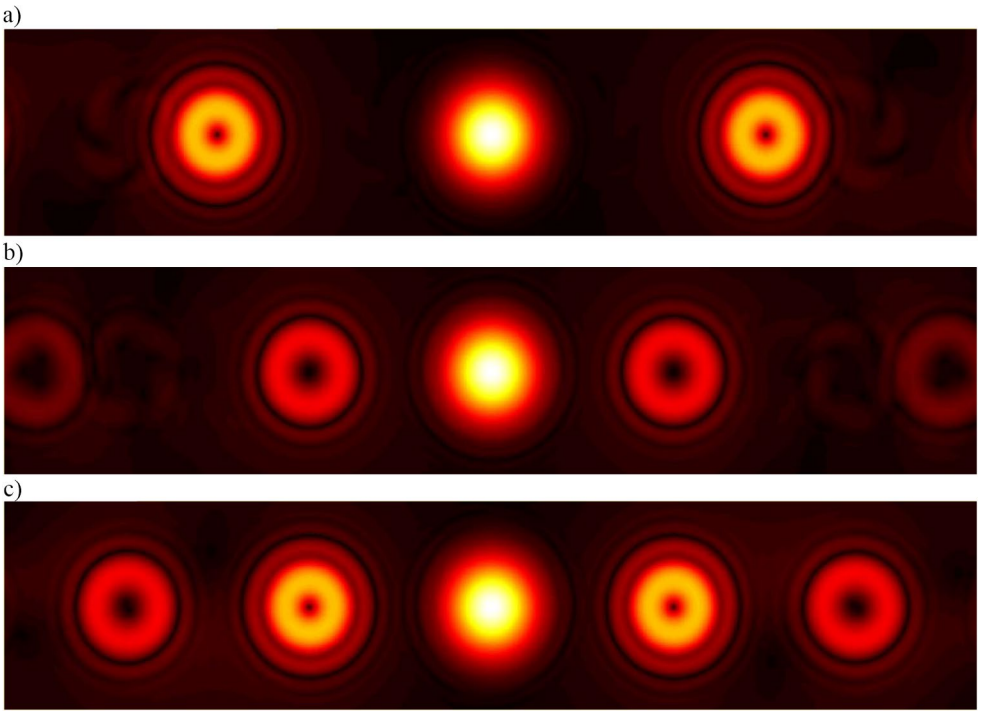


**Fig. 10** Diffraction patterns of a single-branch fork-shaped grating for the groove distances of (**a**) 20 μm, (**b**) 50 μm and (**c**) 100 μm

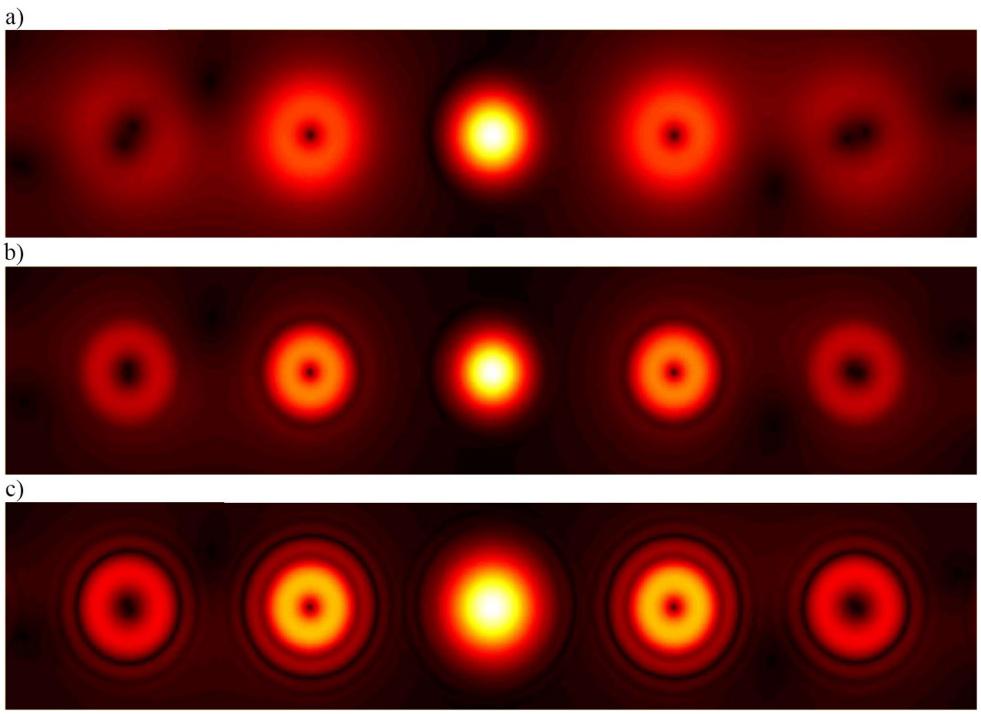


**Fig. 11** Diffraction patterns of a single-branch fork-shaped grating for the Gaussian beam waist sizes of (**a**) 0.5 mm, (**b**) 1 mm and (**c**) 1.5 mm. The groove distance of the grating is kept constant at 100 μm during the simulations

## Conclusion

In this paper, a simple, low-cost, and reproducible method for the preparation of fork-shaped diffraction gratings is presented. The generation of Laguerre–Gaussian beams by the prepared gratings has also been confirmed. Considering the success of the presented simple method in the generation of these types of beams, it can be more optimized to be able to further reduce the groove distance of the prepared gratings through employing other higher resolution printing methods. For example, optical lithography can be used to transfer the designed gratings by the computer-generated holography method on transparent plates or glasses. The generated optimized Laguerre–Gaussian beams can be used in the fields of optical telecommunications and free space optical communications. Moreover, other types of diffraction

gratings can also be prepared by the presented method for the generation of other structured optical beams, such as Top Hat, Bessel-Gaussian, and Hermit-Gaussian beams. The designed computer-generated holograms can be transferred to spatial light modulators to be able to generate these structured light beams in real-time.

**Funding** The authors did not receive support from any organization for the submitted work.

## Declarations

**Financial interests** The authors declare they have no financial interests.

**Non-financial interests** None.

## References

1. A.E. Willner, H. Huang, Y. Yan, Y. Ren, N. Ahmed, G. Xie, C. Bao, L. Li, Y. Cao, Z. Zhao, Optical communications using orbital angular momentum beams. Adv. Opt. Photonics. **7**, 66–106 (2015)
2. G. Gibson, J. Courtial, M.J. Padgett, M. Vasnetsov, V. Pas'ko, S.M. Barnett, S. Franke-Arnold, Free-space Inform. Transf. Using Light Beams Carr. Orbital Angular Momentum Opt. Express. **12**, 5448–5456 (2004)
3. J.H. Poynting, The wave motion of a revolving shaft, and a suggestion as to the angular momentum in a beam of circularly polarised light. Proc. R. Soc. Lond. A, 82, 560-7 (1909)
4. Y. Wang, L. Bai, C. Huang, J. Xie, D. Zhang, L. Guo, Orbital angular momentum of Laguerre-Gaussian beams with non-zero radial index at limited aperture size. Results Phys. **48**, 106436 (2023)
5. L. Allen, M.W. Beijersbergen, R. Spreeuw, J. Woerdman, Orbital angular momentum of light and the transformation of Laguerre-Gaussian laser modes. Phys. Rev. A **45**, 8185 (1992)
6. M. Beijersbergen, R. Coerwinkel, M. Kristensen, J. Woerdman, Helical-wavefront laser beams produced with a spiral phase plate. Opt. Commun. **112**, 321–327 (1994)
7. L. Marrucci, C. Manzo, D. Paparo, Optical spin-to-orbital angular momentum conversion in inhomogeneous anisotropic media. Phys. Rev. Lett. **96**, 163905 (2006)
8. V.Y. Bazhenov, M. Soskin, M. Vasnetsov, Screw dislocations in light wavefronts. J. Mod. Opt. **39**, 985–990 (1992)
9. C. Xu, X. Chen, Y. Cai, Y. Wang, High-quality tunable optical vortex arrays with multiple states of orbital angular momentum. Opt. Laser Technol. **169**, 110029 (2024)
10. H. Fathi, M. Närhi, R. Barros, R. Gumenyuk, Coherent beam combining of optical vortices. Opt. Lett. **49**, 3882–3885 (2024)
11. J. Du, Z. Quan, K. Li, J. Wang, Optical vortex array: generation and applications. Chin. Opt. Lett. **22**, 020011 (2024)
12. X. Jiang, A. Wang, J. Yao, R. Chen, Measuring high-order multiple vortex beams with fork-shaped grating. Optik **257**, 168742 (2022)
13. N. Kumar, A. Arora, A. Krishnan, Single-shot generation of composite optical vortex beams using hybrid binary fork gratings. Opt. Express. **29**, 33703–33715 (2021)
14. S. Sato, H. Inaba, Optical trapping and manipulation of microscopic particles and biological cells by laser beams. Opt. Quantum Electron. **28**, 1–16 (1996)
15. E. Higurashi, H. Ukita, H. Tanaka, O. Ohguchi, Optically induced rotation of anisotropic micro-objects fabricated by surface micromachining. Appl. Phys. Lett. **64**, 2209–2210 (1994)
16. A. Mair, A. Vaziri, G. Weihs, A. Zeilinger, Entanglement Orbital Angular Momentum States Photons Nat. **412**, 313–316 (2001)
17. B. Thidé, H. Then, J. Sjöholm, K. Palmer, J. Bergman, T. Carozzi, Y.N. Istomin, N. Ibragimov, R. Khamitova, Utilization of photon orbital angular momentum in the low-frequency radio domain. Phys. Rev. Lett. **99**, 087701 (2007)
18. P.J. Christopher, R. Mouthaan, B. Wetherfield, E.J. Medcalf, T.D. Wilkinson, Computer-generated Holography Intermediate Domain JOSA A **39**, 392–400 (2022)
19. A.M. Beigzadeh, R. Vaziri, M.R. Ziaie, F., S. Sharif, A new optical method for online monitoring of the light dose and dose profile in photodynamic therapy. Lasers Surg. Med. **52**, 659–670 (2020)
20. W. Burger, M.J. Burge, Digital Image Processing: An Algorithmic Introduction. Springer, pp. 3–28 (2022)
21. Y. Altman, export_fig. [GitHub](https://github.com/altmany/export_fig/releases/tag/v3.27). Retrieved June 14, 2022 (2022)
22. A.V. Carpentier, H. Michinel, J.R. Salgueiro, D. Olivieri, Making optical vortices with computer-generated holograms. Am. J. Phys. **76**, 916–921 (2008)
23. A. Beigzadeh, M.R. Vaziri, F. Ziaie, Z. Soltani, Double-exposure holographic interferometry for radiation dosimetry: a newly developed model. Radiat. Meas. **119**, 132–139 (2018)